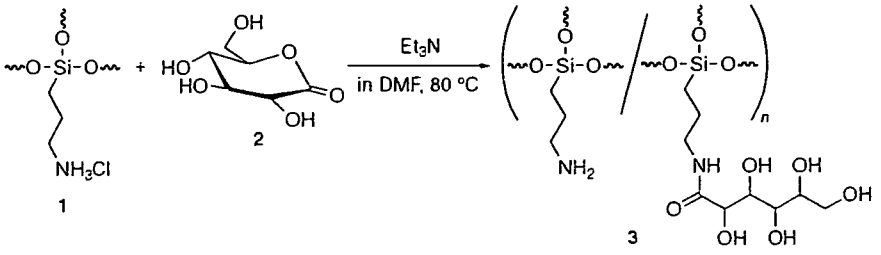

1 2 3

Scheme 1.

In this paper, we describe the synthesis of sugar-polysiloxane hybrids having rigid main-chains by the reaction of sugar-lactones with **1**. Furthermore, we prepared an amphiphilic sugar-polysiloxane hybrid by introduction of long alkyl chains in addition to sugar-residues on the surface of **1** to promote the formation of the nano aggregates in water, expecting the multivalent effects.

EXPERIMENTAL

Materials

The polysiloxane **1** was prepared according to the literature procedure.[11] *N,N*-Dimethylformamide (DMF), dimethyl sulfoxide (DMSO), and triethylamine were purified by distillation. Other reagents were used as received.

Reaction of 1 with Gluconolactone 2[13]

To a suspension of **1** (0.147 g, 1.0 mmol unit) in DMF (2.5 mL) was successively added triethylamine (0.15 mL, 1.1 mmol) and a solution of **2** (0.891 g, 5.0 mmol) in DMF (10 mL) with vigorously stirring at 80 °C under argon. After the mixture was stirred further at that temperature for 13 h, the obtained product was isolated by filtration, washed with DMF and acetone, and then dried under reduced pressure at 40 °C to yield 0.191 g of the yellow-powdered **3**. ^{1}H NMR (600 MHz, D_2O): δ 4.38–4.26 (br, -C(=O)-C*H*-), δ 4.16–4.05 (br, -C(=O)CH(OH)C*H*-), δ 3.88–3.60 (br, -C*H*(OH)C*H*(OH)CH_2-), δ 3.41–3.10 and 3.06–2.91 (br, -NCH_2-), δ 1.88–1.45 (br, -NCH$_2$CH_2-CH$_2$Si-), δ 0.94–0.47 (br, -CH_2Si-).

Synthesis of Hydrophilic Sugar-Polysiloxane Hybrid (5)

To a suspension of **1** (0.147 g, 1.0 mmol unit) in DMSO (3.0 mL) was successively added triethylamine (0.34 mL, 2.4 mmol) and a solution of **4** (1.701 g, 5.0 mmol) in DMSO (10 mL) with vigorously stirring at 80 °C under argon, and the mixture was stirred further at that temperature for 2 h. The mixture became gradually homogeneous solution. The solution was poured into acetone (300 mL) to precipitate the powdered product. The precipitated product was isolated by filtration, successively washed with acetone, hydrochloric acid (HCl) methanol solution and methanol, and then dried under reduced pressure at 40 °C to yield 0.332 g of the light yellow-powdered **5**. ^{1}H NMR (600 MHz, D_2O): δ 4.65–4.50 (br, -OC*H*-(CH-)O-), δ 4.50–4.32 (br, -C(=O)C*H*(OH)-), δ 4.32–4.13 (br, -C(=O)CH(OH)C*H*(OH)-), δ 4.08–3.49 (br, -C*H*(O-)C*H*(OH)CH_2OH, -C*H*(OH)C*H*(OH)C*H*(OH)-C*H*(O-)CH_2OH), δ 3.40–3.12 (br, -C(=O)NHCH_2-), δ 3.12–2.87 (br, Cl·NH$_3$CH_2-), δ 1.95–1.43 (br, -NCH$_2$CH_2CH$_2$Si-), δ 0.93–0.50 (br, -CH_2Si-).

Synthesis of Stearoyl-Carrying Polysiloxane (7)

To a solution of **1** (0.440 g, 3.0 mmol unit) in water (10 mL) was successively added triethylamine (1.0 mL, 7.2 mmol) and a solution of stearoyl chloride (**6**) (0.182 g, 0.6 mmol) in DMF (30 mL) with vigorously stirring at room temperature, and the solution was stirred further at that temperature for 10 min. After 5 mol/L HCl aqueous solution (2.88 mL, 14.4 mmol) was added to this mixture and this solution was stirred further for 5 min, the solution was poured into acetone (300 mL) to precipitate the powdered product. The precipitated product was isolated by filtration, washed with acetone and chloroform, and then dried under reduced pressure at 40 °C to yield 0.437 g of the white-powdered **7**. ^{1}H NMR (600 MHz, DMSO-d_6-D_2O): δ 3.09–2.72 (br, -NCH_2-), δ 2.20–2.01 (br, -C(=O)CH_2-), δ 1.88–1.55 (br, -NCH$_2$CH_2-CH$_2$Si-), δ 1.50–1.40 (br, -C(=O)CH$_2$CH_2-), δ 1.28–1.10 (br, -CCH_2C-), δ 0.95–0.45 (br, -CH$_3$, -CH_2Si-).

Synthesis of Amphiphilic Sugar-Polysiloxane Hybrid (8)

To a solution of **7** (0.150 g, 1.3 mmol unit) in DMSO (5 mL) was successively added triethylamine (0.46 mL, 3.3 mmol) and a solution of **4** (2.212 g, 6.5 mmol) in DMSO (15 mL) with stirring at 80 °C, and the solution was stirred further at that temperature for 2 h. The solution was poured into acetone (300 mL) to precipitate the powdered product. The precipitated product was isolated by filtration, successively washed with acetone, HCl methanol solution and

methanol, and then dried under reduced pressure at 40 °C to yield 0.270 g of the light yellow-powdered **8**. ^{1}H NMR (600 MHz, DMSO-d_6-D_2O): δ 4.46–4.28 (br, -OC*H*(CH-)O-), δ 4.28–4.11 (br, -C(=O)C*H*-(OH)-), δ 4.11–3.95 (br, -C(=O)CH(OH)C*H*(OH)-), δ 3.90–3.28 (br, -C*H*(O-)C*H*(OH)C*H*$_2$OH, -C*H*(OH)-C*H*(OH)C*H*(OH)C*H*(O-)C*H*$_2$OH, overlapped with HOD signal), δ 3.28–2.96 (br, -C(=O)NHC*H*$_2$-), δ 2.96–2.70 (br, Cl·NH$_3$C*H*$_2$-), δ 2.20–2.01 (br, -C(=O)-C*H*$_2$-), δ 1.80–1.32 (br, -NCH$_2$C*H*$_2$CH$_2$Si-, -C(=O)-CH$_2$C*H*$_2$-), δ 1.28–1.13 (br, -CC*H*$_2$C-), δ 0.88–0.80 (br, -CH$_3$), δ 0.80–0.36 (br, -C*H*$_2$Si-).

Measurements

The IR spectra were recorded using a SHIMADZU FT/IR-8400 spectrometer. The ^{1}H NMR spectra (600 MHz) were recorded using a JEOL ECA600 spectrometer. The gel permeation chromatographic (GPC) analyses were performed by using a TOSOH CCPD with RI detector under the following conditions: Shodex GF-310 column with water as the eluent at a flow rate of 0.5 mL/min. The calibration curve was obtained using pullulan standards. The X-ray diffraction (XRD) measurements were conducted at a scanning speed of $2\theta = 0.2°$/min using a RINT 1200 (Rigaku Co., Ltd) diffractometer with Ni-filtered CuKα radiation ($\lambda = 0.15418$ nm). The scanning electron microscope (SEM) images were obtained using a Hitachi S-4100 electron microscope. The dynamic light scattering (DLS) measurement was performed on a Zetasizer 3000 (Malvern Instruments).

RESULTS AND DISCUSSION

Reaction of 1 with 2

As previously reported,[13] an introduction of **2** to **1** was performed by heating at 80 °C in the presence of triethylamine in DMF to prepare a rigid polysiloxane **3** having polyol moieties (Scheme 1). The obtained product **3** was soluble in water and DMSO, but insoluble in typical organic solvents such as methanol, acetone, chloroform, and *n*-hexane.

The IR spectrum of the product showed an absorption at 1150 cm^{-1} attributed to the Si-O bond of the polysiloxane, an absorption at 1080 cm^{-1} assigned to the C-O bond of the polyol moiety derived from **2**, and an absorption at 1650 cm^{-1} due to the C=O bond of the amido group. In addition, the ^{1}H NMR spectrum in D_2O of the product showed both signals due to **1** and **2**. Furthermore, a methylene signal (δ 3.41–3.10) neighboring the amido group was appeared at lower magnetic field compared with a signal (δ 3.06–2.91) neighboring the unreacted amino group. These spectroscopic results indicated that the product has the structure **3** connecting **1** with **2** by the covalent bonds. The functionality of **2** to **1** was calculated to be *ca.* 75% based on the integrated ratio of the methylene signal neighboring the amido group to the methylene signal neighboring the silicon atom.

The molecular weights of **3** and **1** were evaluated by GPC analyses with water as the eluent. The GPC peak of **3** was shifted to the range of higher molecular weight compared to that of **1**. The M_n values of **3** and **1** estimated using pullulan standards were 21,200 g/mol ($M_w/M_n = 1.33$) and 10,300 g/mol ($M_w/M_n = 1.41$), respectively.

The XRD profile of **3** showed three peaks with the *d*-value ratio of $1:1/\sqrt{3}:1/2$ assigned to the (100), (110), and (200) peaks, respectively, indicating that the product has a hexagonal phase. Additionally, the *d*-value of the (100) peak of **3** ($d = 1.76$ nm) was larger than that of **1** ($d = 1.41$ nm). This indicates that the hexagonal phase in solid state was maintained in spite of the increase in the *d*-value by introduction of **2** to **1**.

The above analytical data indicated that **2** efficiently reacted with the amino groups in **1**, giving rise to **3**. To introduce the sugar moieties such as galactose residues on the surface of **1** by means of this reaction manner, the following experiments were performed using lactobionolactone **4**.

Synthesis of Hydrophilic Sugar-Polysiloxane Hybrid 5

We investigated synthesis of galactose-functionalized polysiloxane hybrid **5** by the reaction of **4** with **1**. Procedures for synthesis of **5** were almost same as those of **3**. Since the reaction in DMF gave the insoluble product, however, we employed DMSO as the alternative solvent, which was favorable for this reaction system. When an introduction of **4** to **1** was performed by heating at 80 °C in the presence of triethylamine in DMSO (Scheme 2), the initial reaction system was heterogeneous, which gradually became homogeneous with progress of the reaction. After the product was isolated as the fraction insoluble in acetone, unreacted amino groups were converted to ammonium cations by addition of HCl methanol solution in order to increase solubility and stability of the product in water. The obtained product **5** was soluble in water and DMSO, but insoluble in typical organic solvents such as methanol, acetone, chloroform, and *n*-hexane.

The IR spectrum of the product showed absorptions at 1650 cm^{-1} attributed to the C=O bond of the amido group, indicating the introduction of **4** to **1**. The ^{1}H NMR spectrum in D_2O of the product in Figure 1 shows both signals derived from **1** and **4**. Furthermore, a methylene signal $\mathbf{H_c}$ neighboring the amido group appeared at lower magnetic field compared with a signal $\mathbf{H_{c'}}$ neighboring the unreacted amino group. These spectroscopic data support the structure **5** of

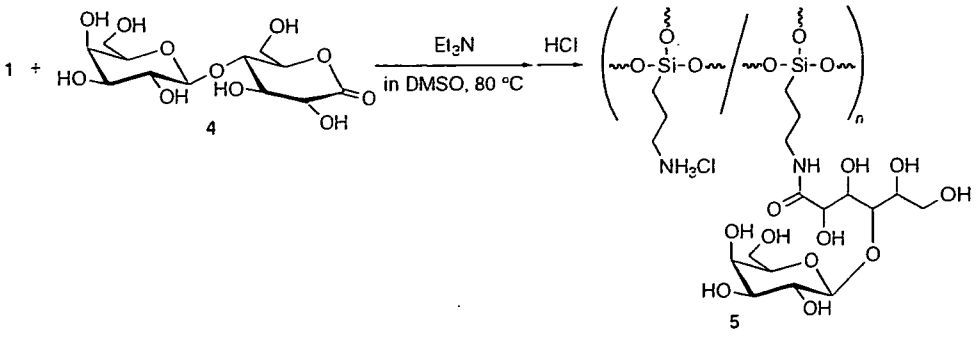

Scheme 2.

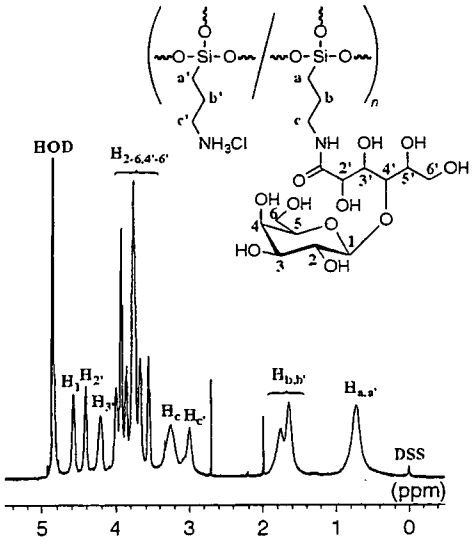

Figure 1. ^{1}H NMR spectrum of **5** in D_2O. Chemical shifts were referenced to sodium 2,2-dimethyl-2-silapentane-5-sulfonate (DSS) (δ 0.0 ppm).

the product. The functionality of **4** to **1** was calculated by the integrated ratio of the signal $\mathbf{H_1}$ to the signals $\mathbf{H_a}$ and $\mathbf{H_{a'}}$ in Figure 1 to be *ca.* 57%. Although the XRD profile of **3** showed three peaks for a typical hexagonal phase as described above, no diffraction peak was observed for **5**, indicating that a regular higher-ordered structure was not formed in the solid state. This would be because that the bulkiness of **4** affected the higher-ordered structure of **5**. However, **5** probably has the rigid structure in the solution due to the Si-O-Si network structure of the main-chain derived from trifunctional organoalkoxysilane. The molecular weight (M_n) of **5** estimated by GPC analysis with water as the eluent using pullulan standards was 44,700 g/mol (M_w/M_n = 1.44).

Synthesis of Amphiphilic Sugar-Polysiloxane Hybrid 8

To promote the formation of the nano aggregates of sugar-polysiloxane hybrid, we attempted synthesis of an amphiphilic hybrid **8** by introduction of the hydrophobic stearoyl groups in addition to the hydrophilic sugar groups on the surface of **5**. However, the reaction of **5** with stearoyl chloride **6** did not proceed to obtain **8**, probably due to bulkiness of sugar-residues existed on the surface of **5**. As an alternative reaction manner, an introduction of **6** to **1** was firstly carried out in the presence of triethylamine in water/DMF mixed solvent at room temperature to produce stearoyl-carrying polysiloxane **7** (Scheme 3). After addition of HCl aqueous solution to this reaction solution, the product was isolated as the fraction insoluble in acetone. The obtained product **7** was soluble in DMSO, but insoluble in water.

The IR spectrum of the product showed an absorption at 1640 cm^{-1} assigned to the C=O bond of the amido group. In addition, the ^{1}H NMR spectrum in DMSO-d_6 (including a small amount of D_2O) of the product in Figure 2 shows both signals derived from **1** and **6**. These spectroscopic results indicate the intro-

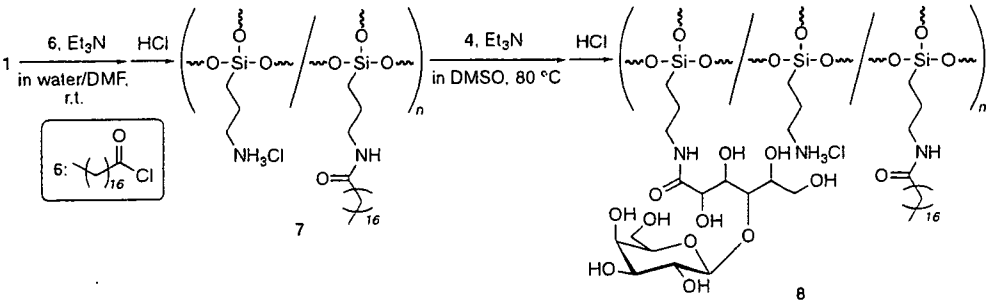

Scheme 3.

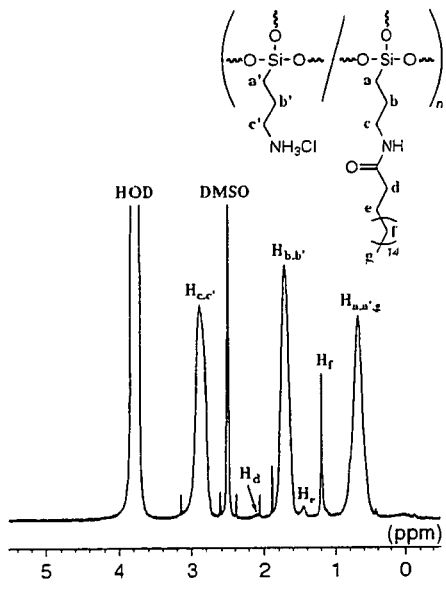

Figure 2. ^{1}H NMR spectrum of **7** in DMSO-d_6 (including a small amount of D_2O). Chemical shifts were referenced to DMSO (δ 2.5 ppm).

duction of **6** to **1**, leading to **7**. The functionality of **6** to **1** was calculated to be *ca.* 2% based on the integrated ratio of the signal $\mathbf{H_f}$ to the signal $\mathbf{H_b}$ and $\mathbf{H_{b'}}$. When the feed ratio of **6** to **1** was increased, the insoluble product was obtained.

As a second step, we carried out a reaction of **4** with **7** by heating at 80 °C in the presence of triethylamine in DMSO to obtain amphiphilic sugar-polysiloxane hybrid **8** (Scheme 3). The product was isolated as the fraction insoluble in acetone, followed by washing with acetone, HCl methanol solution, and methanol. The obtained product **8** was soluble in water and DMSO, but insoluble in typical organic solvents such as methanol, acetone, chloroform, and *n*-hexane.

The IR spectrum of the product showed an absorption at 1140 cm^{-1} attributed to the Si-O bond, an absorption at 1080 cm^{-1} assigned to the C-O bond of **4**, and an absorption at 1650 cm^{-1} due to the C=O bond of the amido group. Additionally, the ^{1}H NMR spectrum in DMSO-d_6 (including a small amount of D_2O) of the product in Figure 3a shows signals derived from **1**, **4**, and **6**. Furthermore, the methylene signals $\mathbf{H_a}$ and $\mathbf{H_b}$ of the product shift to higher field and the methylene signal $\mathbf{H_c}$ shifts to lower field compared with those of **7**. These shifts have also been observed in the synthesis of **3**,[13] and are attributed to progress of the amidation reaction of **7** with **4**. These spectroscopic results fully support the structure of the sugar- and stearoyl-functionalized polysiloxane **8**. The functionality of **4** to **1** was calculated by the integrated ratio of the signal $\mathbf{H_{f'}}$ to the signal $\mathbf{H_1}$ in Figure 3 to be *ca.* 48%, when the reaction was carried out under the conditions as described in experimental sec-

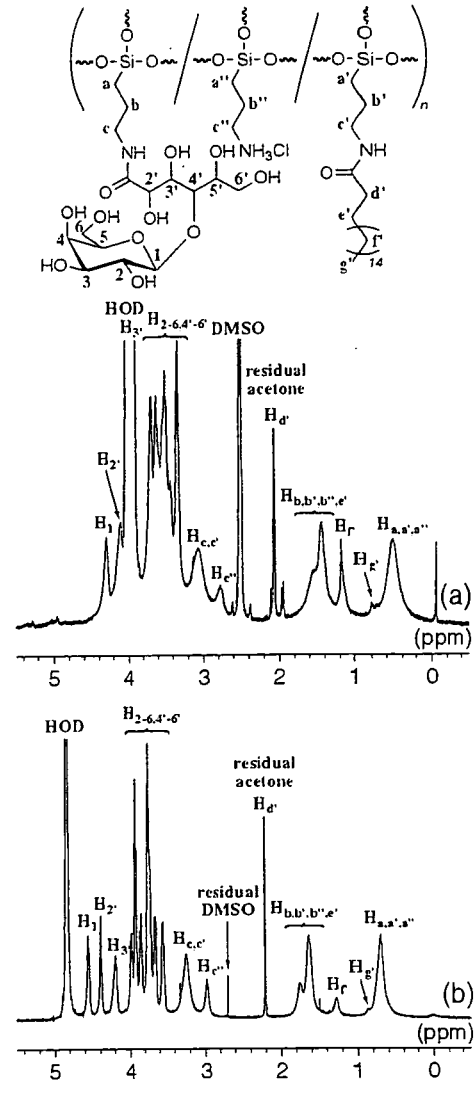

Figure 3. ^{1}H NMR spectrum of **8** (a) in DMSO-d_6 (including a small amount of D_2O) and (b) in D_2O. Chemical shifts were referenced to DMSO (δ 2.5 ppm) and DSS (δ 0.0 ppm), respectively.

tion. The functionalities were variable by changing the feed ratio of **4** to **7**.

Interestingly, intensity of a signal $\mathbf{H_{f'}}$ due to stearoyl group of **8** in D_2O decreases compared with that in DMSO-d_6 (Figure 3b). This observation indicates that the stearoyl groups existed in the inside of the intra and intermolecular aggregates of **8** in D_2O. To confirm the formation of nano aggregates of **8** in water, SEM image of **8** was taken. The SEM specimen was prepared by evaporating an aqueous solution of **8** on a spinning aluminium plate. The SEM image of the surface of **8** coated on the aluminum plate shows that nano aggregates were formed from **8** (Figure 4); nano aggregates having the particle diameters of *ca.* 50 nm are appearing at high frequency and larger particles that represent a diameter of *ca.* 500 nm are coexisting with smaller aggregates at much lower frequency (a few aggregates in a SEM image). The particle size

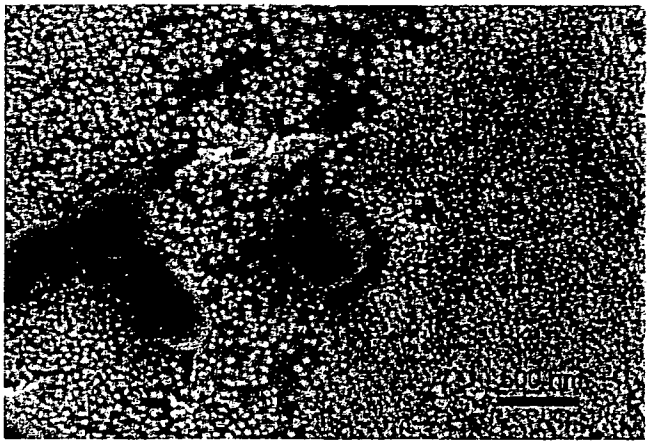

Figure 4. SEM image of **8**.

was also confirmed by dynamic light scattering (DLS) measurement. The mean diameter of the particle composed of **8** was 67.7 ± 4.5 nm (poly dispersity index: 0.273) in water. The aggregate size corresponds well to that was observed in the SEM image of the spin-coating sample of **8**.

CONCLUSIONS

The amino groups existed on the surface of the rigid polysiloxane (**1**) efficiently reacted with gluconolactone (**2**) to give the corresponding hybrid (**3**). This reaction manner was employed for preparation of the hydrophilic sugar-polysiloxane hybrid (**5**), which was achieved by the reaction of **1** with lactobionolactone (**4**). Furthermore, the amphiphilic sugar-polysiloxane hybrid (**8**) was also derived from **1** by the successive reactions with stearoyl chloride (**6**) and with **4**. The obtained hybrid materials **5** and **8** have galactose residues on their surfaces. Although hybrid **3** had the regular higher-ordered structure in the solid state, hydrophilic sugar-polysiloxane hybrid **5** did not form such a structure by the bulkiness of **4**. However, amphiphilic sugar-polysiloxane hybrid **8** formed the nano aggregates in water, which was confirmed by the ^{1}H NMR, SEM, and DLS analyses, expecting the multivalent effects of sugar-residues. The present materials are new class of sugar-inorganic hybrids, which have rigid polysiloxane main-chains.

Acknowledgment. The author (T.N.) thanks Dr. Tetsuji Yamaoka and Dr. Atsushi Mahara of National Cardiovascular Center for dynamic light scattering measurement.

REFERENCES

1. M. Okada, *Prog. Polym. Sci.*, **26**, 67 (2001).
2. K. Kobayashi, A. Tsuchida, T. Usui, and T. Akaike, *Macromolecules*, **30**, 2016 (1997).
3. X. L. Sun, K. M. Faucher, M. Houston, D. Grande, and E. L. Chaikof, *J. Am. Chem. Soc.*, **124**, 7258 (2002).
4. Q. Wang, J. S. Dordick, and R. J. Linhardt, *Chem. Mater.*, **14**, 3232 (2002).
5. A. B. Lowe, B. S. Sumerlin, and C. L. McCormick, *Polymer*, **44**, 6761 (2003).
6. L. Albertin, M. Stenzel, C. Barner-Kowollik, L. J. R. Foster, and T. P. Davis, *Macromolecules*, **37**, 7530 (2004).
7. G. Jonas and R. Stadler, *Acta. Polym.*, **45**, 14 (1994).
8. V. Braunmühl, G. Jonas, and R. Stadler, *Macromolecules*, **28**, 17 (1995).
9. V. Braunmühl and R. Stadler, *Polymer*, **39**, 1617 (1998).
10. K. Loos, G. Jonas, and R. Stadler, *Macromol. Chem. Phys.*, **202**, 3210 (2001).
11. Y. Kaneko, N. Iyi, K. Kurashima, T. Matsumoto, T. Fujita, and K. Kitamura, *Chem. Mater.*, **16**, 3417 (2004).
12. Y. Kaneko, N. Iyi, T. Matsumoto, and K. Kitamura, *Polymer*, **46**, 1828 (2005).
13. Y. Kaneko, J. Kadokawa, M. Setoguchi, and N. Iyi, *Polymer*, **46**, 8905 (2005).

ELSEVIER

NUTRITION

Nutrition 23 (2007) 81–86

www.elsevier.com/locate/nut

Basic nutritional investigation

Kurozu moromimatsu inhibits tumor growth of Lovo cells in a mouse model in vivo

Naoto Fukuyama, M.D., Ph.D.[a,*], Shio Jujo[a], Isao Ito, M.D., Ph.D.[b], Toru Shizuma, M.D., Ph.D.[a], Kazunori Myojin, M.D., Ph.D.[c], Kazuo Ishiwata, Ph.D.[a], Masanobu Nagano, Ph.D.[d], Hiroe Nakazawa, M.D., Ph.D.[a], and Hidezo Mori, M.D., Ph.D.[e]

[a] *Department of Physiology, Tokai University, School of Medicine, Isehara, Kanagawa, Japan*
[b] *Department of Surgery, Tokai University, School of Medicine, Isehara, Kanagawa, Japan*
[c] *Department of Radiology, Tokai University, School of Medicine, Isehara, Kanagawa, Japan*
[d] *Sakamoto Jozo Inc., Kagoshima, Kagoshima, Japan*
[e] *Department of Cardiac Physiology, National Cardiovascular Center, Suita, Osaka, Japan*

Manuscript received June 2, 2006; accepted October 12, 2006.

Abstract

Objective: In Japan, rice vinegar that has been matured and fermented for years in earthenware jars is considered a health food with anticolon cancer action. It is divided into the liquid component (Kurozu) and the sediment (Kurozu moromimatsu), which contains large amounts of organic materials and minerals. The effect of Kurozu moromimatsu (Kurozu-M) on cancer has not yet been examined. In this study, we examined the activity of Kurozu-M on colon cancer and investigated the mechanisms involved, focusing on active oxygen generation, apoptosis, and metalloproteinases (MMPs).

Methods: We used Lovo cells transplanted into nude mice as an experimental model. We measured the tumor volume and MMP levels and conducted hematoxylin-eosin staining (for polymorphonuclear leukocytes), terminal deoxynucleotidyl transferase-mediated dUTP nick end-labeling staining (for apoptosis), and immunostaining for nitrotyrosine (a marker of active oxygen generation) in control, Kurozu-treated, and Kurozu-M—treated groups.

Results: The tumor volume was the same in the control group (231 ± 36 mm^3) and Kurozu group (238 ± 52 mm^3), but was significantly reduced in the Kurozu-M group (152 ± 28 mm^3, $P < 0.001$ versus control). Apoptosis of tumor cells and accumulation of polymorphonuclear leukocytes were not observed. Nitrotyrosine production, total MMP levels, and MMP activation were significantly reduced in the Kurozu-M group.

Conclusion: The administration of Kurozu-M prolonged the lifespan of cancer cell–transplanted mice, inhibited tumor progression, and reduced nitrotyrosine production and MMP activation, but did not induce apoptosis.

Keywords: Kurozu; Kurozu moromimatsu; Lovo cell; Colon cancer

This work was supported by grants from Tokai University School of Medicine Research Aid in 2004, 2005, and 2006; the research and study program of Tokai University Educational System General Research Organization; the Kanagawa Nanbyou Foundation in 2004; Grants-in-Aid for Scientific Research in 2003 (grant 15659285), 2005 (grant 17659375), and 2006 (grant 18390336) from the Ministry of Education, Science and Culture, Japan; Health and Labour Sciences Research Grants for Research on Human Genome, Tissue Engineering Food Biotechnology in 2003 (grant H15-saisei-003); Health and Labour Sciences Research Grants for Comprehensive Research on Cardiovascular Diseases in 2004 (grant H16-jyunkannki[seishuu]-009) and 2006 (grant H18-jyunkannki[seishuu]-ippan-018); and Health and Labour Science Research Grants for research on medical devices for analyzing, supporting, and substituting the function of human body in 2005 (grant H17-physi-002).

* Corresponding author. Tel.: +81-463-931-121; fax: +81-463-936-684.
E-mail address: fukuyama@is.icc.u-tokai.ac.jp (N. Fukuyama).

0899-9007/07/$ – see front matter
doi:10.1016/j.nut.2006.10.004

Introduction

In Japan, rice vinegar is widely used in the preparation of Sushi or Kaisekiryouri. It is known to have a bactericidal action and an orexigenic action and was reported to have a preventive effect against hypertension and arterial sclerosis [1]. Recently, rice vinegar that has been matured and fermented for many years in earthenware jars has attracted attention as a health food. The supernatant is known as Korozu, and the solid residue of the production process, Kurozu moromimatsu (Kurozu-M), is rich in organic materials and minerals. However, the effect of Kurozu-M on disease has not yet been examined.

Colorectal cancer accounts for >90% of malignant tumors of the large intestine and is the third most common cause of death from malignant disease in the Western world [2]. It was reported that ethyl acetate extract of Kurozu inhibited carcinogenesis in azoxymethane-treated rats [3] and caused G0/G1 arrest through p21 induction in Caco-2 cells [4]. It is known that active oxygen species activate metalloproteinases (MMPs) in colon cancer tissue, leading to destruction of the basal membrane [5], thereby promoting distant metastasis. However, the effects of Kurozu on active oxygen production and MMP activation are unknown.

In this study, we examined the direct effects of Kurozu and Kurozu-M on human colon cancer cells (DLD cells, well-differentiated adenocarcinoma; Lovo cells, poorly differentiated adenocarcinoma) transplanted into nude mice and found that both inhibited tumor growth. We also examined the mechanisms involved, focusing on active oxygen production and MMP activation. Because direct measurement of active oxygen production in tissues is difficult, we used an indirect method based on staining for nitrotyrosine, the formation of which involves active oxygen.

Materials and methods

Preparation of Kurozu and Kurozu-M diets

The Kurozu and Kurozu-M diets were obtained from Sakamotojyozo Co., Ltd. (Kagoshima, Japan). The Kurozu diet included 0.32% 10-fold–concentrated Kurozu, and the Kurozu-M diet included 2% Kurozu moromimatsu powder in CE-2 basic rodent diet (Nihon CLEA Co., Ltd, Tokyo, Japan).

Preparation of animal model

Lovo and DLD cells were maintained under the conditions recommended by the supplier. Four-week-old to 6-wk-old female nude mice were maintained in a pathogen-free environment and handled according to the university's guidelines for animal care and use.

Female nu/nu mice were injected with 1×10^6 Lovo cells or DLD cells into the right flank. The tumors reached 5–10 mm in diameter at about 6 wk after injection in the control group on a standard CE-2 diet. The CE-2, Kurozu, or Kurozu-M diet was supplied from 1 wk before cancer cell injection.

Measurement of subcutaneous tumor

Tumor dimensions were measured with a linear caliper every 2 or 3 days for one month. We measured the major axis and the tumor volume, which was calculated using the equation $V\ (mm^3) = a \times b^2$, where a is the largest dimension and and b is the perpendicular diameter.

Hematoxylin-eosin staining, terminal deoxynucleotidyl transferase-mediated dUTP nick end-labeling staining, and nitrotyrosine immunostaining

At the end of the experiment, tumor tissue was fixed with 4% paraformaldehyde and sectioned. Hematoxylin-eosin (HE) staining was performed with conventional methods. Terminal deoxynucleotidyl transferase-mediated dUTP nick end-labeling (TUNEL) staining was performed according to the kit manufacturer's instructions, and apoptosis was visualized as brown staining, located in the nucleus. Apoptotic cells were counted in 10 fields of each slide under a 40× microscope.

For nitrotyrosine staining, endogenous peroxidase in sections was quenched with 0.3% H_2O_2 in 60% methanol for 30 min. The sections were permeabilized with 0.1% Triton X-100 in phosphate buffered saline (PBS) for 20 min. Nonspecific adsorption was minimized by incubating the sections in 2% normal goat serum in PBS for 20 min. Sections were incubated overnight with anti-nitrotyrosine rabbit polyclonal antibody (1:500 in PBS), and specific labeling was detected with diaminobenzidine tetrahydrochloride. To verify the binding specificity to nitrotyrosine, some sections were incubated with primary antibody only (no secondary antibody) or with secondary antibody only (no primary antibody). No positive staining was found in these sections, indicating that the immunoreaction was specific. Some sections were incubated with the primary antibody (anti-nitrotyrosine) in the presence of excess nitrotyrosine (10 mM) to further verify the binding specificity.

MMP-2 and MMP-9 assays

Levels of total MMP-2 and MMP-9 and endogenous activated MMP-2 and MMP-9 were assayed with commercial assay kits (Amersham Pharmacia Biotech, Buckinghamshire, UK).

MMP-2 assay

Eight weeks after injection of Lovo cells, tumors were removed. Tissues were homogenized in 50 mM Tris-HCl buffer (pH 7.4) containing 1 mM monothioglycerol and

centrifuged at 2000 *g* for 10 min. The supernatant was used as the sample. One hundred microliters of each standard blank or sample (in duplicate) was added to wells coated with MMP-2 antibody. The 96-well plate was then incubated overnight at 4°C. Any MMP-2 present within the samples was bound to the wells and other components were removed by washing. All standards and one well for each sample were activated with aminophenylmercuric acetate (APMA, 0.5 mM) to determine total MMP-2 levels, and the remaining wells were incubated with assay buffer alone to determine endogenous activated MMP-2. The detection reagent was then added to each well and the plate was incubated at 37°C for 4 h. After incubation, the absorbance of each well was read at 405 nm on a microplate reader and the concentrations (nanograms per milliliter) of total MMP-2 and endogenous activated MMP-2 were determined for each sample from a standard curve using Revelation Software (Dynatech, UK). Final tissue values were expressed as nanograms per milligram of protein.

MMP-9 assay

Standards and samples were run in the same manner as described for MMP-2 on a microplate coated with MMP-9 antibody, except that 1 mM APMA was used for activation, and incubation with the detection reagent was done at 37°C for 6 h. The absorbance was read with a microplate reader as described for MMP-2. Final tissue values were expressed as nanograms per milligram of protein.

Results

Measurement of subcutaneous tumor

We measured the major axis of the tumor to examine whether the administration of Kurozu or Kurozu-M could inhibit tumor growth. In the DLD cell–transplanted model, the major axes were 8.1 ± 0.5 mm in the control group, 7.90 ± 0.80 mm in Kurozu group, and 7.8 ± 0.80 mm in the Kurozu-M group. There were no significant differences among the three groups (Fig. 1A). However, in the Lovo cell–transplanted model, the major axes of the tumor were 8.2 ± 0.5 mm in the control group and 7.8 ± 0.8 mm in the Kurozu group, but significantly reduced to 6.0 ± 0.8 mm in the Kurozu-M group ($P < 0.05$ versus control; Fig. 1B).

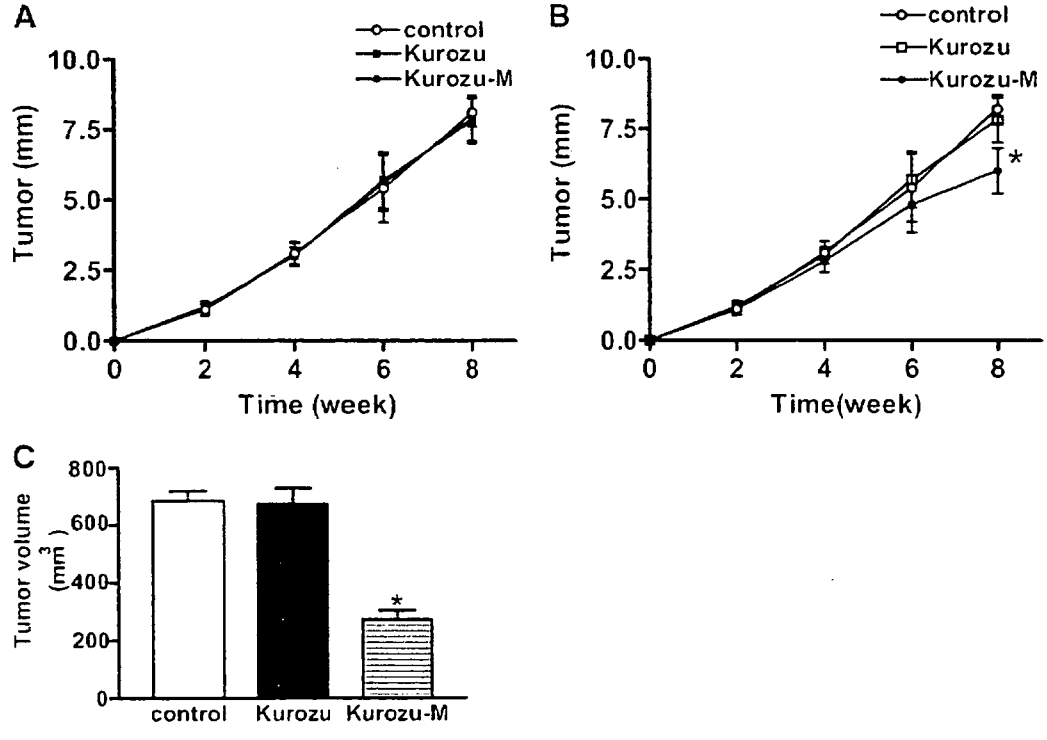

Fig. 1. Antitumor effect of Kurozu and Kurozu moromimatsu. Female nu/nu mice were injected with 1 × 10^6 Lovo cells or DLD cells into the right flank. (A) Time course of tumor growth in DLD-1 cell–transplanted mice (long diameter). Open circles represent the control group, solid squares the Kurozu-treated group, and solid circles the Kurozu moromimatsu–treated group. (B) Time course of tumor growth in Lovo cell–transplanted mice (long diameter). Open circles indicate the control group, open squares the Kurozu-treated group, and solid circles the Kurozu moromimatsu–treated group. (C) Tumor volume in Lovo cell–transplanted mice. Tumor volume was measured 8 wk after Lovo cell inoculation. The open bar indicates the control group, the solid bar the Kurozu-treated group, and the horizontally lined bar the Kurozu moromimatsu–treated group. Values are means ± SD. *$P < 0.001$ versus other groups.

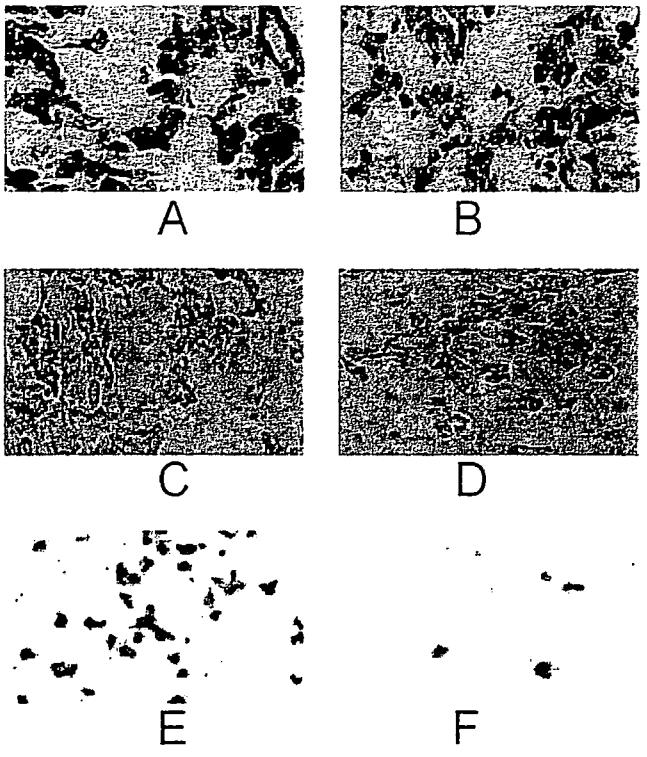

Fig. 2. Histologic examination of cancerous tissue after Lovo cell transplantation. Hematoxylin-eosin staining of tumor from (A) the control group and (B) the Kurozu moromimatsu–treated group. Terminal deoxynucleotidyl transferase-mediated dUTP nick end-labeling staining of tumor from (C) the control group and the (D) Kurozu moromimatsu–treated group. Nitrotyrosine staining of tumor from (E) the control group and (F) the Kurozu moromimatsu–treated group.

In the Lovo cell–transplanted model, the tumor volumes were 684.0 ± 34.0 mm^3 in the control group, 672.0 ± 56.0 mm^3 in the Kurozu group, and 273.0 ± 32.0 mm^3 in the Kurozu-M group ($P < 0.005$ for the Kurozu-M group versus control; Fig. 1C).

The following results refer to the Lovo cell–transplanted model.

HE staining, TUNEL staining, and nitrotyrosine immunostaining

The HE staining showed no accumulation of polymorphonuclear leukocytes, which have been implicated in active oxygen production, in tumor tissue in the control group or the Kurozu-M group (Fig. 2A,B).

The TUNEL staining indicated that apoptosis in the Kurozu-M group was at the same level as that in the control group (Fig. 2C,D).

Because we previously found that nitrotyrosine, generated from peroxynitrite and tyrosine, is produced in human colon cancer [5], we examined whether the administration of Kurozu-M could inhibit nitrotyrosine formation. In the control group, many cells produced nitrotyrosine, whereas in the Kurozu-M group, only a few cells produced nitrotyrosine (Fig. 2E,F).

MMP-2 and MMP-9 assays

To investigate the role of MMPs in the action of Kurozu-M, we examined whether or not Kurozu-M altered the levels and activation of MMPs.

Total MMP-2 amounted to 8.8 ± 2.5 ng/mg of protein in the control group and 8.6 ± 2.8 ng/mg of protein in the Kurozu group. However, it was significantly reduced to 5.6 ± 1.8 ng/mg of protein by administration of Kurozu-M ($P < 0.05$ versus control; Fig. 3A). Activated MMP-2 amounted to 0.25 ± 0.06 ng/mg of protein in the control group, 0.27 ± 0.08 ng/mg of protein in the Kurozu group, and 0.12 ± 0.05 ng/mg of protein in the Kurozu-M group ($P < 0.05$ for the Kurozu-M group versus control; Fig. 3A).

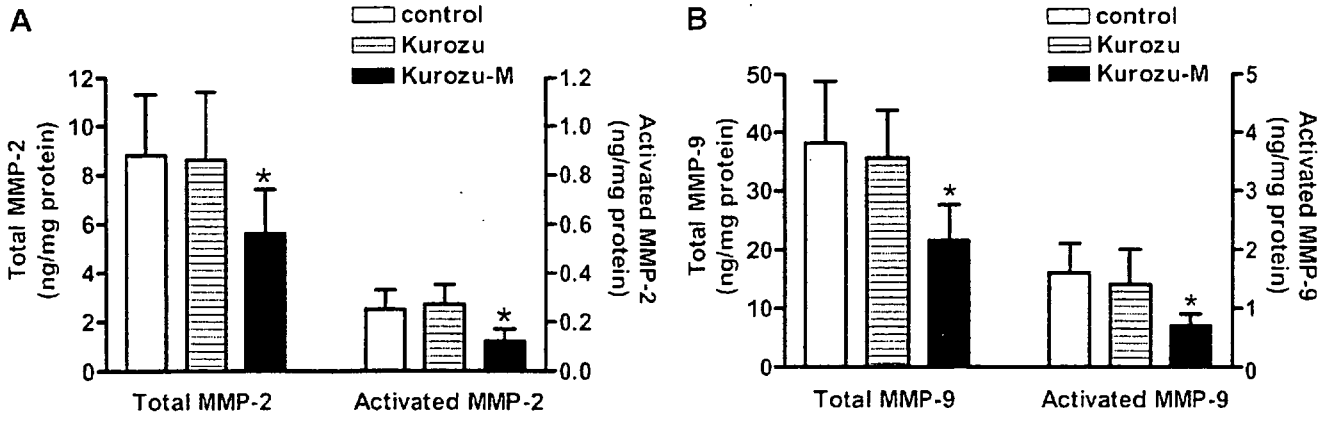

Fig. 3. Anti-metalloproteinase effect of Kurozu and Kurozu moromimatsu. (A) Total and activated metalloproteinase-2 in cancerous tissue after Lovo cell inoculation. The open bar represents the control group, the horizontally lined bar the Kurozu-treated group, and the solid bar the Kurozu moromimatsu-treated group. (B) Levels of total and activated metalloproteinase-9 in cancerous tissue after Lovo cell inoculation. The open bar represents the control group, the horizontally lined bar the Kurozu-treated group, and the solid bar the Kurozu moromimatsu–treated group. Values are means ± SD. *$P < 0.001$ versus other groups.

Total MMP-9 amounted to 38.2 ± 10.6 ng/mg of protein in the control group and 35.6 ± 8.22 ng/mg of protein in the Kurozu group. However, it was significantly reduced to 21.5 ± 6.1 ng/mg of protein by administration of Kurozu-M ($P < 0.05$ versus control; Fig. 3B). Activated MMP-9 amounted to 1.6 ± 0.5 ng/mg of protein in the control group, 1.4 ± 0.6 ng/mg of protein in the Kurozu group, and 0.7 ± 0.2 ng/mg of protein in the Kurozu-M group ($P < 0.05$ for the Kurozu-M group versus control; Fig. 3B).

Discussion

Our results indicate that the administration of Kurozu-M inhibits the development of colon cancer in human colon cancer cell transplantation model in mice. Further, the administration of Kurozu-M inhibited nitrotyrosine production, decreased total MMP-2 and total MMP-9 levels, and inhibited activation of MMP-2 and MMP-9 in the lesion in this model.

Earlier studies had indicated that extract of Kurozu can inhibit chemical carcinogenesis [3,4,6]. However, in our study, the administration of Kurozu-M inhibited the development of colon cancer in a mouse model, whereas the administration of Kurozu did not prevent tumor growth. The major constituent of Kurozu is acetic acid, whereas the major component of Kurozu-M is a complex mixture of organic materials, including bacterial metabolites. The active components of Kurozu-M remain to be identified.

In this study, we found that administration of Kurozu-M inhibited production of nitrotyrosine in tumor tissue. Nitrotyrosine is generated through two pathways in vivo. One is the peroxynitrite pathway, in which tyrosine reacts with peroxynitrite to afford nitrotyrosine, and the second is the myeloperoxidase pathway, in which tyrosine reacts with myeloperoxidase and nitrite [7,8]. We previously reported that peroxynitrite is produced in human colon cancer tissue [5]. In contrast, myeloperoxidase is localized in polymorphonuclear leukocytes in vivo, but in this study we could not detect any accumulation of polymorphonuclear leukocytes by means of HE staining of cancerous tissue. Therefore, Kurozu-M administration may inhibit the peroxynitrite pathway. Possible mechanisms include inhibition of nitric oxide, superoxide, and/or peroxynitrite production, and scavenging of nitric oxide, superoxide, and/or peroxynitrite. Further work is needed to examine these possibilities.

The administration of Kurozu-M also inhibited MMP-2 and MMP-9 activity in cancerous tissue. These are representative gelatinases that contribute to the distant metastasis of cancer [9], and they are produced by cancer cells or macrophages [10]. A tetradecanoylphorbol acetate-responsive element is present in the promoter region of MMP-9 and is activated by various cytokines, such as interleukin and tumor necrosis factor [11]. In addition, MMP-9 is activated by nuclear factor-κB and MMP-2 [12]. MMP-2 is mainly activated by MT1-MMP, but recently it was shown that peroxynitrite also activates MMP-2 [13,14]. Kurozu-M may have inhibited cancer growth in our model through inhibition of peroxynitrite formation and MMP-2 and MMP-9 activities.

Kurozu moromimatsu was active against Lovo cells in this study, but not against DLD-1 cells. Lovo and DLD-1 cells differ not only in the degree of cellular differentiation but also in the expression of furin, which contributes to MMP activation [15]. The former line originates from well-differentiated adenocarcinoma and expresses furin protein, whereas the latter originates from poorly differentiated adenocarcinoma and does not express furin protein. It would be worth examining whether MMP activity is reduced in the absence of furin.

Conclusion

The administration of Kurozu-M inhibited tumor growth in a Lovo cell–transplanted mouse model and also inhibited nitrotyrosine production and activation of MMP-2 and MMP-9.

References

[1] Shimoji Y, Tamura Y, Nakamura Y, Nanda K, Nishidai S, Nishikawa Y, et al. Isolation and identification of DPPH radical scavenging compounds in Kurosu (Japanese unpolished rice vinegar). J Agric Food Chem 2002;50:6501–3.

[2] Shen X, Falzon M. PTH-related protein enhances LoVo colon cancer cell proliferation, adhesion, and integrin expression. Regul Pept 2005; 125:17–27.

[3] Shimoji Y, Kohno H, Nanda K, Nishikawa Y, Ohigashi H, Uenakai K, et al. Extract of Kurosu, a vinegar from unpolished rice, inhibits azoxymethane-induced colon carcinogenesis in male F344 rats. Nutr Cancer 2004;49:170–3.

[4] Nanda K, Miyoshi N, Nakamura Y, Shimoji Y, Tamura Y, Nishikawa Y, et al. Extract of vinegar "Kurosu" from unpolished rice inhibits the proliferation of human cancer cells. J Exp Clin Cancer Res 2004;23: 69–75.

[5] Szaleczky E, Pronai L, Nakazawa H, Tulassay Z. Evidence of in vivo peroxynitrite formation in patients with colorectal carcinoma, higher plasma nitrate/nitrite levels, and lower protection against oxygen free radicals. J Clin Gastroenterol 2000;30:47–51.

[6] Shimoji Y, Sugie S, Kohno H, Tanaka T, Nanda K, Tamura Y, et al. Extract of vinegar "Kurosu" from unpolished rice inhibits the development of colonic aberrant crypt foci induced by azoxymethane. J Exp Clin Cancer Res 2003;22:591–7.

[7] Eiserich JP, Hristova M, Cross CE, Jones AD, Freeman BA, Halliwell B, et al. Formation of nitric oxide-derived inflammatory oxidants by myeloperoxidase in neutrophils. Nature 1998;391:393–7.

[8] Fukuyama N, Takebayashi Y, Hida M, Ishida H, Ichimori K, Nakazawa H. Clinical evidence of peroxynitrite formation in chronic renal failure patients with septic shock. Free Radic Biol Med 1997; 22:771–4.

[9] Gullu IH, Kurdoglu M, Akalin I. The relation of gelatinase (MMP-2 and -9) expression with distant site metastasis and tumour aggressiveness in colorectal cancer. Br J Cancer 2000;82:249.

[10] Djonov V, Cresto N, Aebersold DM, Burri PH, Altermatt HJ, Hristic M, et al. Tumor cell specific expression of MMP-2 correlates

with tumor vascularisation in breast cancer. Int J Oncol 2002; 21:25–30.

[11] Steinbrenner H, Ramos MC, Stuhlmann D, Mitic D, Sies H. Brenneisen P. Tumor promoter TPA stimulates MMP-9 secretion from human keratinocytes by activation of superoxide-producing NADPH oxidase. Free Radic Res 2005;39:245–53.

[12] Wittrant Y. Theoleyre S, Couillaud S, Dunstan C, Heymann D, Redini F. Relevance of an in vitro osteoclastogenesis system to study receptor activator of NF-kB ligand and osteoprotegerin biological activities. Exp Cell Res 2004;293:292–301.

[13] Munoz-Najar UM. Neurath KM, Vumbaca F, Claffey KP. Hypoxia stimulates breast carcinoma cell invasion through MT1-MMP and MMP-2 activation. Oncogene 2005.

[14] Migita K, Maeda Y, Abiru S, Komori A, Yokoyama T, Takii Y, et al. Peroxynitrite-mediated matrix metalloproteinase-2 activation in human hepatic stellate cells. FEBS Lett 2005;579:3119–25.

[15] Deryugina EI, Ratnikov BI, Yu Q, Baciu PC, Rozanov DV, Strongin AY. Prointegrin maturation follows rapid trafficking and processing of MT1-MMP in Furin-negative colon carcinoma LoVo cells. Traffic 2004;5:627–41.

Basic Res Cardiol 102:209–216 (2007)
DOI 10.1007/s00395-006-0629-9

ORIGINAL CONTRIBUTION

Naoto Fukuyama
Etsuro Tanaka
Yasuhiko Tabata
Hisanori Fujikura
Masao Hagihara
Hiromi Sakamoto
Kiyoshi Ando
Hiroe Nakazawa
Hidezo Mori

Intravenous injection of phagocytes transfected ex vivo with FGF4 DNA/biodegradable gelatin complex promotes angiogenesis in a rat myocardial ischemia/reperfusion injury model

Received: 18 April 2006
Returned for 1. revision: 21 June 2006
1. Revision received: 11 September 2006
Accepted: 9 October 2006
Published online: 27 October 2006

N. Fukuyama (✉) · H. Fujikura · M. Hagihara · K. Ando · H. Nakazawa
Depts. of Physiology, Internal Medicine and Center for Regenerative Medicine
Tokai University School of Medicine
Isehara, 259-1193, Japan
Tel.: +81-463/93-1121
Fax: +81-463/93-6684
E-Mail: fukuyama@is.icc.u-tokai.ac.jp

E. Tanaka
Dept. of Nutritional Sciences
Tokyo University of Agriculture
Tokyo, Japan

Y. Tabata
Research Center for Biomedical Engineering
Kyoto University
Kyoto, Japan

H. Sakamoto
Genetics Division
National Cancer Center Research Institute
Tokyo, Japan

H. Mori
National Cardiovascular Center Research Institute
Suita, Japan

Abstract Conventional gene therapies still present difficulties due to poor tissue-targeting, invasiveness of delivery, method, or the use of viral vectors. To establish the feasibility of using non-virally ex vivo transfected phagocytes to promote angiogenesis in ischemic myocardium, gene-transfection into isolated phagocytes was performed by culture with positively charged gelatin impregnated with plasmid DNA. A high rate of gene transfection was achieved in rat macrophages and human monocytes, but not in mouse fibroblasts. The efficiency was 68 ± 11 % in rat macrophages and 78 ± 8 % in human monocytes. Intravenously injected phagocytes accumulated predominantly in ischemic tissue (13 ± 8 %) and spleen (84 ± 6 %), but negligibly in other organs in rodents. The efficiency of accumulation in the target ischemic tissue reached more than 86 % on direct local tissue injection. In a rat model of myocardial ischemia-reperfusion, intravenous injection of fibroblast growth factor 4 (FGF4)-gene-transfected macrophages significantly increased regional blood flow in the ischemic myocardium (78 ± 7.1 % in terms of flow ratio of ischemic/non-ischemic myocardium) compared with intravenous administration of saline (36 ± 11 %) or non-transfected macrophages (42 ± 12 %), or intramuscular administration of naked DNA encoding FGF4 (75 ± 18 %). Enhanced angiogenesis in the ischemic tissue we confirmed histologically. Similarly, intravenous injection of FGF4-gene-transfected monocytes enhanced regional blood flow in an ischemic hindlimb model in mice (93 ± 22 %), being superior to the three other treatments described above (38 ± 12, 39 ± 15, and 55 ± 12 %, respectively).

Phagocytes transfected ex vivo with FGF4 DNA/gelatin promoted angiogenesis. This approach might have potential for non-viral angiogenic gene therapy.

Key words angiogenesis - cells - gene therapy - growth substances - ischemia

Abbreviations and acronyms

ANOVA = analysis of variance
FGF4 = fibroblast growth factor-4
GFP = green fluorescent protein
pI = isoelectric point

Introduction

Conventional gene therapies still require improvement with regard to transfection efficiency and safety [1, 2], as well as tissue targeting [3], despite recent advances. Achievement of a high transfection rate often requires a viral vector, but the safety of the viruses has not yet been

Basic Research in Cardiology, Vol. 102, No. 3 (2007)
© Steinkopff Verlag 2006

established [4–6]. Conventional non-viral vectors seem to be inferior to viral ones in transfection efficiency, except for nucleofection [7, 8]. Conventional gene therapy using a viral vector can induce inflammation in the gene-transduced tissue [9]. Moreover, in vivo gene-delivery to the localized target tissue usually necessitates invasive approaches. For example, direct gene-transfection to cardiomyocytes requires surgical operation [10] or cardiac catheterization [11, 12]. On the other hand, ex vivo gene-transfection is less invasive, but tissue-targeting by intravenous injection is difficult to achieve [3].

Macrophages accumulate in ischemic tissue based on the mechanism of immune response (chemotaxis) [13]. This suggests that intravenous transplantation of macrophages may target the ischemic tissue in vivo. Tabata et al. previously reported that gelatin particles are phagocytized by macrophages [14, 15]. The isoelectric point (pI) of gelatin can be changed by modification of its residues, and positively charged gelatin can be impregnated with negatively charged substances [16] such as nucleic acid [17]. Thus, gelatin may be suitable as a vector for transfecting phagocytes ex vivo.

We describe here a study aimed at examining the feasibility of a new concept for less invasive, cell-based gene therapy, by means of ex vivo gene transfection into isolated phagocytes (macrophages and monocytes) using a non-viral vector, gelatin, followed by intravenous injection of the transfected phagocytes. The present method has significant advantages over conventional cell-based gene delivery [18, 19], in that the intravenously injected cells (phagocytes) not only produce protein from the transfected gene, but have a tissue-targeting ability.

Methods

This study was performed in accordance with the Guideline of Tokai University School of Medicine on Animal Use, which conforms to the NIH Guide for the Care and Use of Laboratory Animals (DHEW publication No. (NIH) 86-23, Revised 1985, Offices of Science and Health Reports, DRR/NIH, Bethesda, MD 20205).

Animals

A total of 121 Fisher rats (male, 10 weeks old, Clea Japan Inc., Tokyo) and 61 nude SCID mice (male, 6 weeks old, Shizuoka Animal Center, Shizuoka, Japan) were used. Rats were anesthetized by inhalation of diethyl ether for harvesting macrophages and with isofluren (1.5–3 %) for thoracotomy, after which they were mechanically ventilated with a mixture of oxygen and nitrous oxide. Mice were anesthetized by intraperitoneal injection of sodium pentobarbital (40 mg/kg).

A model of myocardial ischemia-reperfusion injury was prepared in 41 rats. The remaining 80 rats were used for collecting activated macrophages. The heart was exposed via thoracotomy, and the proximal left anterior descending coronary artery was ligated [20] for 180 min, followed by reperfusion. A model of hindlimb ischemia was prepared in 61 mice. The left femoral artery was ligated and resected [21].

Cells

Macrophages were obtained from 80 rats. Thioglycolate (4 %, 8 ml) was injected into the peritoneal cavity, and after 4 days, peritoneal macrophages were collected [22]. Monocytes were obtained from peripheral blood of healthy volunteers. Leukocyte-rich plasma was obtained by dextran 500 sedimentation and layered onto Nycoprep 1.068 (Nycomed, Birmingham, UK). The monocyte-containing layer was aspirated, washed twice and allowed to adhere to the dish for 90 minutes. Fibroblasts (NIH 3T3, Invitrogen Corporation, Carlsbad, CA) were also used. The cells were resuspended in RPMI 1640 medium (Sigma) containing 5 % heat-inactivated fetal calf serum and cultured for 7–14 days. The cell viability and type were determined by trypan blue exclusion and by immunostaining using anti-macrophage antibody up to 14 days.

Genes and vector

Complementary DNA (cDNA) of green fluorescent protein (GFP), Renilla luciferase or human hst1/FGF4 (FGF4) [17] was inserted into the expression vector pRC/CMV (Invitrogen Corporation, Carlsbad, CA) and the constructs were designated as pRC/CMV-GFP, pRC/CMV-luciferase and pRC/CMV-HST1-10, respectively. Preparation and purification of the plasmid from cultures of pRC/CMV-GFP-, pRC/CMV-luciferase-, or pRC/CMV-HST1-10-transformed *Escherichia coli* were performed by equilibrium centrifugation in cesium chloride-ethidium bromide gradients.

Gelatin was prepared from porcine skin [14]. After swelling in water the gelatin particles used in this study were spheroids with a diameter of approximately 5–30 μm, water content of 95 %, and pI of 11. Gelatin (2 mg) was incubated with 50 μg of the plasmid for 7 days at 4 °C to make a gelatin-DNA complex [14].

Experimental protocols

Ex vivo gene transfection Macrophages, monocytes, and fibroblasts (1×10^6) were cultured with the gelatin-DNA complex (2 mg of gelatin plus 50 μg of DNA) for 14 days on a culture dish (100 mm in diameter). Gene ex-

pression of GFP was evaluated by fluorescence microscopy and fluorescence-activated cell sorting. Luciferase activity in the cell lysate was evaluated with a photon counter system after cell lysis [23].

Organ distribution of phagocytes injected intravenously and directly into ischemic muscle To examine tissue-targeting by intravenous injection of transfected phagocytes, the distribution of the cells into organs was evaluated by immunohistochemistry. In the rat model of myocardial ischemia-reperfusion injury, the GFP-gene-transfected macrophages (1.0×10^6 each) were injected into the superficial dorsal vein of the penis at the initiation of reperfusion ($n = 7$ and 5, respectively). In the mouse model of hindlimb ischemia, the GFP-gene-transfected monocytes (1.0×10^6) were injected into the caudal vein 14 days after induction of ischemia ($n = 5$). To examine the tissue-targeting by direct local injection of transfected phagocytes, the distribution of the cells into organs was also evaluated. In the rat model of myocardial ischemia-reperfusion injury ($n = 7$) and the mouse model of hindlimb ischemia ($n = 5$), the same numbers of transfected macrophages and monocytes were directly injected into ischemic myocardium and ischemic skeletal muscle, respectively. Tissue samples were obtained 24 hours after cell administration. Each tissue was homogenized and cytospin was performed. Immunohistochemical analysis was done with anti-GFP antibody (CLONTECH, USA. GFP-monoclonal antibody). GFP positive macrophages were counted in each tissue and expressed as a percentage of total GFP-positive cells.

Amelioration of ischemia by intravenous injection of angiogenic gene-transfected phagocytes The angiogenic effect of intravenously injected FGF4-gene-transfected phagocytes on the ischemia models was evaluated. In the rat model of myocardial ischemia-reperfusion injury, FGF4-gene-transfected macrophages ($n = 5$), non-transfected macrophages (1.0×10^6 each) ($n = 5$), or saline ($n = 5$) were injected into the superficial dorsal vein of the penis, or naked FGF4-DNA (50 μg) was injected directly into the ischemic myocardium ($n = 5$), at the initiation of reperfusion. Fourteen days after the cell administration, blood flows in the ischemic and non-ischemic regions in the heart were evaluated with a noncontact laser Doppler flowmeter (FLO-N1, Omegawave Corporation). Then, tissue samples were obtained and histological analysis was performed. In a mouse model of hindlimb ischemia, just after induction of ischemia, FGF4-gene-transfected monocytes ($n = 15$), non-transfected monocytes ($n = 8$) (1.0×10^6 each), or saline ($n = 10$) were injected into the caudal vein, or naked FGF4-DNA (50 μg) was injected directly into the ischemic muscle ($n = 12$). Fourteen days after induction of ischemia, blood flows in the limbs were evaluated with the noncontact laser Doppler flowmeter (FLO-N1, Omegawave Corporation).

Histology

Ten micrometer sections were cut from formalin-fixed, paraffin-embedded tissue. Two sections were used for H.E. staining and azan staining, and eight sections were used for immunohistochemical staining. Immunohistochemical staining was performed by an indirect immunoperoxidase method. Anti-GFP antibody, anti-Mac1 antibody (BMA Biomedicals Ag, Switzerland), and anti-CD31 antibody (Serotec, UK) were used as primary antibodies. Mac1-antigen is specific to macrophages/monocytes. Anti-Ig, peroxidase-linked species-specific F(ab')2 fragments (Amersham Pharmacia Biotech UK Ltd., UK), were used as a secondary antibody. Double staining was performed with alkaline staining and peroxidase staining. The vessel density stained with von Willebrand factor-antibody was calculated by morphometric assessment in one 16 randomly selected fields of each heart and expressed as number/mm^2.

Statistical analysis

Data are presented as mean values ± SD. Differences were assessed by using ANOVA (analysis of variance) with the Scheffe's multiple comparisons test. A value of $P < 0.05$ was considered statistically significant.

Results

Ex vivo gene transfection

We studied whether genes could be transfected into isolated rat macrophages, human monocytes, and mouse fibroblasts ex vivo by using gelatin. Transfection of the GFP gene into isolated rat macrophages (Figs. 1A and B) and human monocytes (Figs. 1C and D), but not into mouse fibroblasts (data not shown), was achieved by culture with gelatin-DNA complex for 14 days. The gene transfection efficiency into rat macrophages was 68 ± 11% (30 experiments, Fig. 2A) and that into human monocytes was 78 ± 8% (30 experiments) as determined with a fluorescence activated cell sorter. Sequential analysis after luciferase-gene transfection into rat macrophages revealed high expression after 14 days of culture (Fig. 2B).

Basic Research in Cardiology, Vol. 102, No. 3 (2007)

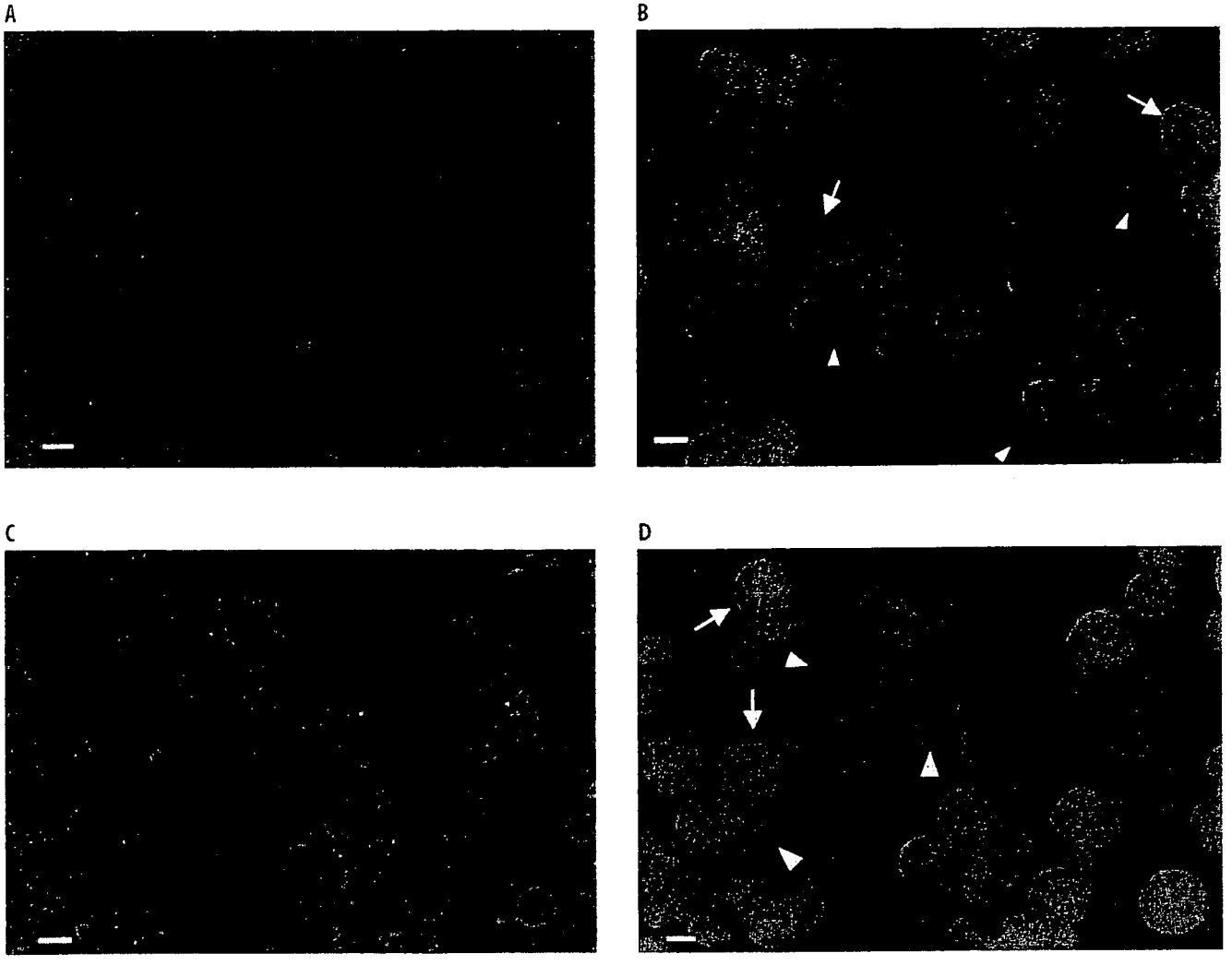

Fig. 1 Fluorescent presentation of ex vivo gene transfection with gelatin-DNA complex in macrophages/monocytes as well as fibroblasts. Rat macrophages (**A** and **B**) and human monocytes (**C** and **D**) were cultured with gelatin-GFP-gene complex for 14 days. Transmittance microscopic images (**A** and **C**) and fluorescence images (**B** and **D**) of the cells are shown. Macrophages (**B**) and monocytes (**D**) show fluorescence due to GFP. Arrowheads indicate GFP-expressing cells. Arrows indicate gelatin particles themselves. Bars = 20 μm

Organ distribution of phagocytes injected intravenously or directly into ischemic muscle

We studied quantitatively whether intravenously injected luciferase-gene-transfected phagocytes could target ischemic tissues (the third and fifth columns from the left in Table 1). In non-ischemic rats, the injected macrophages were recognized almost exclusively in the spleen (98 ± 4 %) (n = 7, the second column in Table 1). In non-ischemic mice, similar results were observed (n = 7, data not shown). In a rat with myocardial ischemia-reperfusion injury, some of the intravenously injected macrophages were incorporated into the heart (the third column in Table 1). The incorporation into the post-ischemic pericardium amounted to 13 ± 6 % (n = 7) (non-ischemic rats 0 ± 0 %, n = 7, Table 1). The incorporated cells expressed GFP (Fig. 3). Fibrosis with inflammatory infiltrates was recognized in the anterior wall of the left ventricle, extending to the interventricular septum (Figs. 3A and B). These infiltrates were mainly polymorphonuclear leukocytes and macrophages (Figs. 3C and D). Approximately 20 % of the macrophages showed GFP-positivity in this area (Figs. 3E and F). Similar tissue-targeting by intravenously injected monocytes was confirmed in a mouse model with hindlimb ischemia (13 ± 7 %, n = 7, the fifth column in Table 1). Furthermore, we studied whether local intramuscular injection increased the degree of tissue targeting (the fourth and sixth columns from the left in Table 1). After direct injection of phagocytes into ischemic muscle, 86 ± 10 % and 88 ± 6 % of the cells remained in the target tissue in the two models. Thirteen and 11 % of phagocytes in-

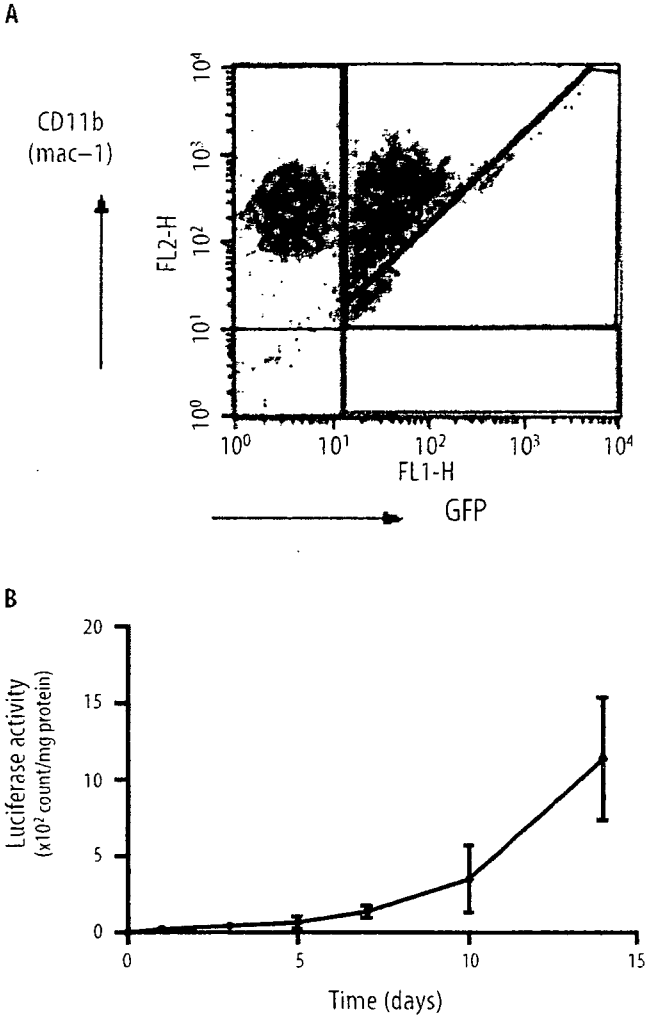

Fig. 2 Quantitative assessment of gene transfection into rat macrophages. (**A**) Fluorescence-activated cell sorting analysis of transfected macrophages done on day 14 of culture with reference to GFP-positive and Mac1-positive cells. (**B**) Sequential changes of luciferase activity in cultured macrophages in the presence of luciferase-gene-gelatin complex. Values are mean ± SD. The number of experiments is shown in parentheses

jected into the cardiac or hindlimb muscle migrated to the spleen. In the other organs, accumulation of phagocytes were negligible.

Amelioration of ischemia by intravenously injected angiogenic-gene-transfected phagocytes

In the rat model with myocardial ischemia-reperfusion injury, we studied the angiogenic effect of intravenously injected macrophages transfected with fibroblast growth factor 4 (FGF4) gene by using gelatin. Intravenous injection of these macrophages (1.0×10^6) significantly increased the regional blood flow in the ischemic myocardium (78 ± 7.1 %, n = 8, in terms of flow ratio of ischemic/non-ischemic myocardium) compared with the other three treatments ($P < 0.05$, ANOVA), that is, intravenous administration of saline (35 ± 10 %, n = 8), intramuscular administration of naked DNA encoding FGF4 (50 μg, direct intramyocardial injection after thoracotomy) (58 ± 5.3 %, n = 8), and intravenous administration of the same number of non-transfected macrophages (42 ± 12 %, n = 8) (Fig. 4A). Histological analyses revealed angiogenesis in the ischemic tissue after the administration of transfected cells (Figs. 4B and C). Similar results were observed in the mouse model with hindlimb ischemia. Intravenous injection of FGF4-gene-transfected monocytes (1.0×10^6) enhanced regional blood flow in the ischemic leg (Fig. 4D). The increase of blood flow in the mice with transfected monocytes (93 ± 22 % in terms of flow ratio of ischemic/non-ischemic leg) was significantly larger than those obtained with the other three treatments described above (38 ± 12, 55 ± 12, and 39 ± 15 %, $P < 0.05$, ANOVA). Neither lymph node swelling in any part of the body nor pathologic change in the spleen or lung, such as angioma or abnormal immune response, was found in any of the animals.

Table 1 Organ distribution of phagocytes injected into the vein and into local tissue

Organ	Normal i.v. (7 rats)	Myocardial injury i.v. (7 rats)	Myocardial injury i.m. (7 rats)	Hindlimb ischemia i.v. (7 mice)	Hindlimb ischemia i.m. (7 mice)
Heart	0±0	13±6	86±10	0±0	0±0
Hindlimb muscle	0±0	0±0	0±0	13±7	88±6
Spleen	98±4	84±6	13±10	84±6	11±6
Lung	1±2	1±1	1±2	1±2	1±1
Liver	1±2	1±1	1±1	1±2	1±1
Brain	0±0	0±0	0±0	0±0	0±0
Kidney	0±0	0±0	0±0	0±0	0±0
Intestine	0±0	0±0	0±0	0±0	0±0

Each value shows a distribution ratio (%) into organs of transfected macrophages/monocytes (mean ± SD). *i.v.* intravenous injection into the vein; *i.m.* direct injection into the jeopardized muscle

Discussion

The advantages of the present method are as follows. First, genes can easily be transfected into phagocytes (macrophages/monocytes). In preliminary experiments, we found that genes can also be transfected into endothelial progenitor cells [25]. Compared with other transfection method, the transfection efficiency was high (68 ± 11 %) and it is not necessary to use a potentially hazardous viral vector [2, 26, 32]. Second, the phagocytes can target the pathologic tissues by chemotaxis even after intravenous injection, and higher tar-

Basic Research in Cardiology, Vol. 102, No. 3 (2007)

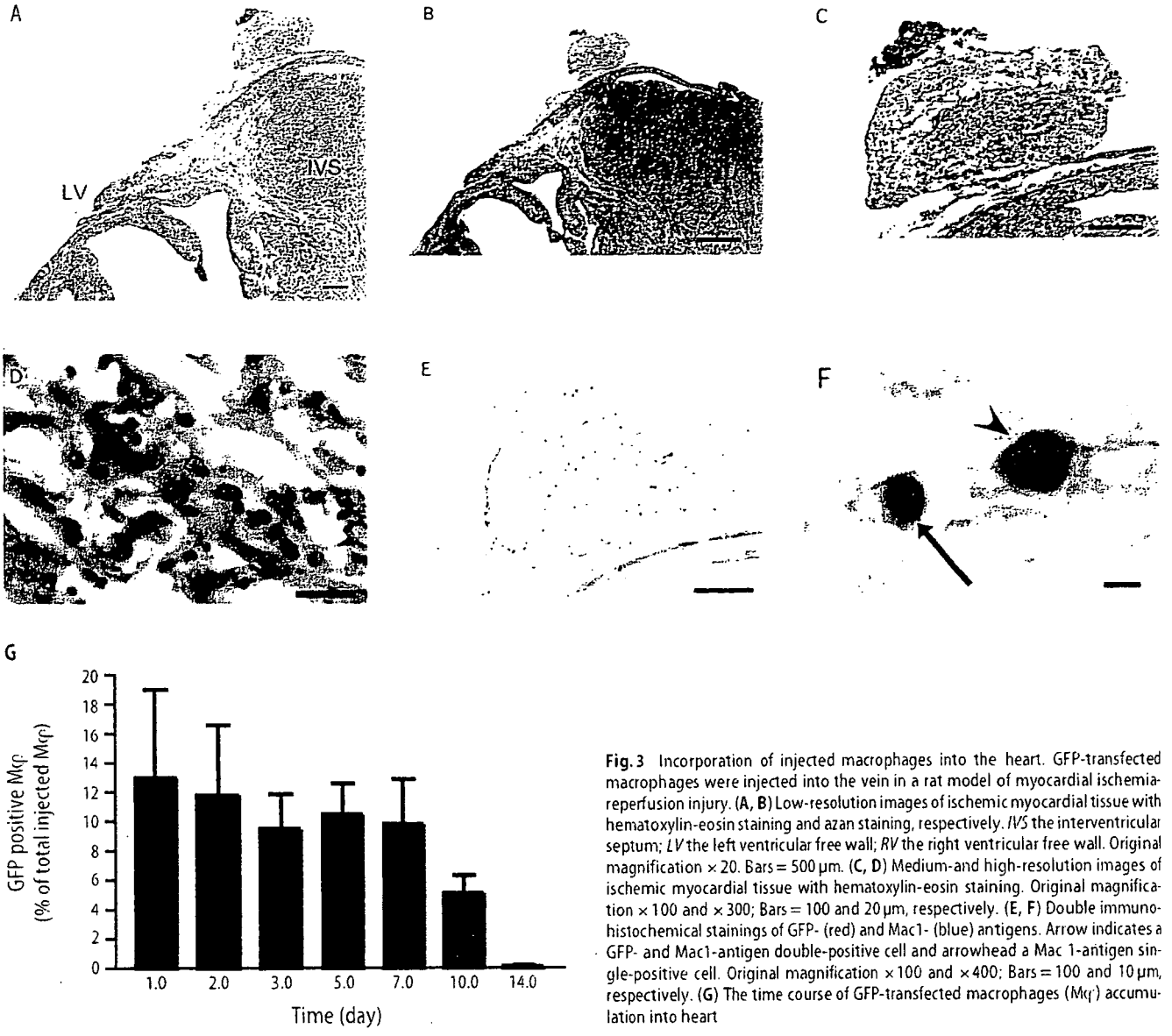

Fig. 3 Incorporation of injected macrophages into the heart. GFP-transfected macrophages were injected into the vein in a rat model of myocardial ischemia-reperfusion injury. (**A, B**) Low-resolution images of ischemic myocardial tissue with hematoxylin-eosin staining and azan staining, respectively. *IVS* the interventricular septum; *LV* the left ventricular free wall; *RV* the right ventricular free wall. Original magnification × 20. Bars = 500 µm. (**C, D**) Medium-and high-resolution images of ischemic myocardial tissue with hematoxylin-eosin staining. Original magnification × 100 and × 300; Bars = 100 and 20 µm, respectively. (**E, F**) Double immunohistochemical stainings of GFP- (red) and Mac1- (blue) antigens. Arrow indicates a GFP- and Mac1-antigen double-positive cell and arrowhead a Mac 1-antigen single-positive cell. Original magnification × 100 and × 400; Bars = 100 and 10 µm, respectively. (**G**) The time course of GFP-transfected macrophages (Mφ) accumulation into heart

geting is available if they are administered locally. The injection is repeatable. We confirmed that the angiogenic gene-transfected phagocytes enhanced angiogenesis after ischemia-reperfusion injury in rat heart and ameliorated ischemia in a mouse hindlimb model.

The injected phagocytes migrated into pathologic tissues, presumably in response to the release of cytokines such as monocyte chemoattractant protein 1 by injured endothelial cells [27]. Adhesion molecules such as P-selectin [28] are probably involved in the recruitment of phagocytes to the vessel wall. The injected phagocytes also migrated to the spleen, but no pathologic change was found in the spleen.

The present method has several advantages over conventional methods of cell-based gene therapy such as fibroblast-based and smooth muscle cell-based approaches [18, 19, 33, 34]. For example, monocytes do not aggregate in vessels, while fibroblasts or smooth muscle cells cannot be injected intravenously because of aggregation. The transfected phagocytes not only synthesize protein from the transfected gene, but also are partially targeted to the impaired tissue. In addition, the transfection rate was better than those of methods such as lipofection, viral vectors and electroporation [26, 29]. The newly developed technique of nucleofection has a transfection efficiency of 40–70 % [30], which is similar to that of our method, but our procedure is easier to use [30, 31]. Further, the therapeutic effect obtained here was superior to that of conventional gene therapy which we reported previously, i.e., intramuscular injection of

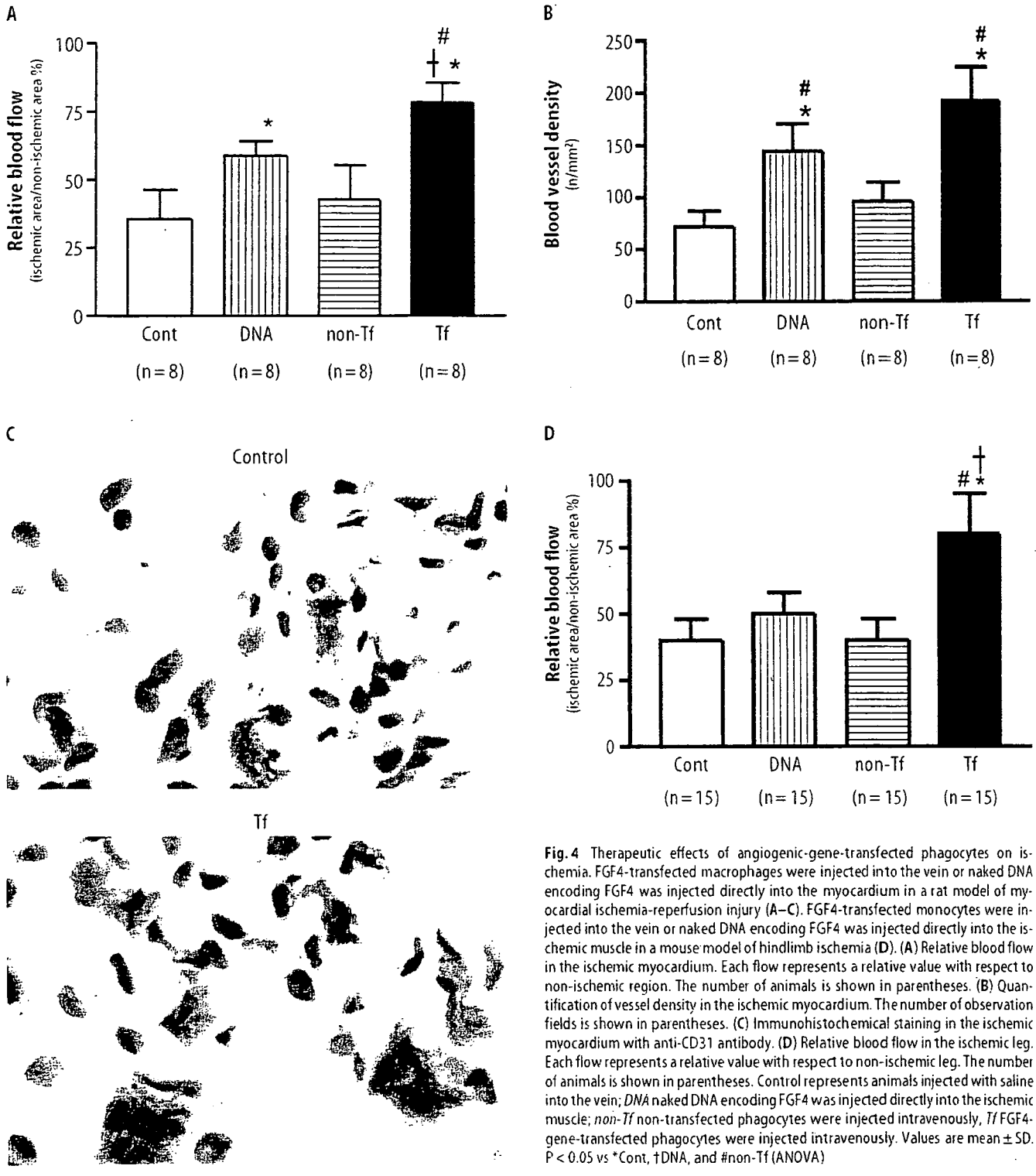

Fig. 4 Therapeutic effects of angiogenic-gene-transfected phagocytes on ischemia. FGF4-transfected macrophages were injected into the vein or naked DNA encoding FGF4 was injected directly into the myocardium in a rat model of myocardial ischemia-reperfusion injury (**A–C**). FGF4-transfected monocytes were injected into the vein or naked DNA encoding FGF4 was injected directly into the ischemic muscle in a mouse model of hindlimb ischemia (**D**). (**A**) Relative blood flow in the ischemic myocardium. Each flow represents a relative value with respect to non-ischemic region. The number of animals is shown in parentheses. (**B**) Quantification of vessel density in the ischemic myocardium. The number of observation fields is shown in parentheses. (**C**) Immunohistochemical staining in the ischemic myocardium with anti-CD31 antibody. (**D**) Relative blood flow in the ischemic leg. Each flow represents a relative value with respect to non-ischemic leg. The number of animals is shown in parentheses. Control represents animals injected with saline into the vein; *DNA* naked DNA encoding FGF4 was injected directly into the ischemic muscle; *non-Tf* non-transfected phagocytes were injected intravenously, *Tf* FGF4-gene-transfected phagocytes were injected intravenously. Values are mean ± SD. $P < 0.05$ vs *Cont, †DNA, and #non-Tf (ANOVA)

naked DNA, in ischemia models of heart and leg [17]. The major disadvantage of our method is the cell preparation time of 2 weeks before therapy can be started, and further work is needed to speed up this process.

Acknowledgements The authors wish to thank Jobu Itoh, Yoshiko Shinozaki, and Takayuki Hasegawa for their technical work.

Basic Research in Cardiology, Vol. 102, No. 3 (2007)

References

1. Pfeifer A, Verma IM (2001) Gene therapy: promises and problems. Annu Rev Genomics Hum Genet 2:177–211
2. Watson DJ, Kobinger GP, Passini MA, Wilson JM, Wolfe JH (2002) Targeted transduction patterns in the mouse brain by lentivirus vectors pseudotyped with VSV, Ebola, Mokola, LCMV, or MuLV envelope proteins. Mol Ther 5:528–537
3. Li Q, Bolli R, Qiu Y, Tang XL, Guo Y, French BA (2001) Gene therapy with extracellular superoxide dismutase protects conscious rabbits against myocardial infarction. Circulation 103: 1893–1898
4. Ferber D (2001) Gene therapy. Safer and virus-free? Science 294:1638–1642
5. Kay MA, Glorioso JC, Naldini L (2001) Viral vectors for gene therapy: the art of turning infectious agents into vehicles of therapeutics. Nat Med 7:33–40
6. Isner JM (2002) Myocardial gene therapy. Nature 415:234–239
7. Nishikawa M, Hashida M (2002) Nonviral approaches satisfying various requirements for effective in vivo gene therapy. Biol Pharm Bull 25:275–283
8. Schakowski F, Buttgereit P, Mazur M, Mazur M, Marten A, Schottker B, Gorschluter M, Schmidt-Wolf IG (2004) Novel non-viral method for transfection of primary leukemia cells and cell lines. Genet Vaccines Ther 2:1
9. Tomasoni S, Benigni A (2004) Gene therapy: how to target the kidney. Promises and pitfalls. Curr Gene Ther 4: 115–122
10. Losordo DW, Vale PR, Symes JF, Dunnington CH, Esakof DD, Maysky M, Ashare AB, Lathi K, Isner JM (1998) Gene therapy for myocardial angiogenesis: initial clinical results with direct myocardial injection of phVEGF165 as sole therapy for myocardial ischemia. Circulation 98:2800–2804
11. Kornowski R, Leon MB, Fuchs S, Vodovotz Y, Flynn MA, Gordon DA, Pierre A, Kovesdi I, Keiser JA, Epstein SE (2000) Electromagnetic guidance for catheter-based transendocardial injection: a platform for intramyocardial angiogenesis therapy. Results in normal and ischemic porcine models. J Am Coll Cardiol 35:1031–1039
12. Laitinen M, Hartikainen J, Hiltunen MO, Eranen J, Kiviniemi M, Narvanen O, Makinen K, Manninen H, Syvanne M, Martin JF, Laakso M, Yla-Herttuala S (2000) Catheter-mediated vascular endothelial growth factor gene transfer to human coronary arteries after angioplasty. Hum Gene Ther 11:263–270
13. Ramsay SC, Weiller C, Myers R, Cremer JE, Luthra SK, Lammertsma AA, Frackowiak RS (1992) Monitoring by PET of macrophage accumulation in brain after ischaemic stroke. Lancet 339:1054–1055
14. Tabata Y, Ikada Y (1987) Macrophage activation through phagocytosis of muramyl dipeptide encapsulated in gelatin microspheres. J Pharm Pharmacol 39: 698–704
15. Tabata Y, Ikada Y (1988) Macrophage phagocytosis of biodegradable microspheres composed of L-lactic acid/glycolic acid homo- and copolymers. J Biomed Mater Res 22:837–858
16. Ikada Y, Tabata Y (1998) Protein release from gelatin matrices. Adv Drug Deliv Rev 31:287–301
17. Kasahara H, Tanaka E, Fukuyama N, Sato E, Sakamoto H, Tabata Y, Ando K, Iseki H, Shinozaki Y, Kimura K, Kuwabara E, Koide S, Nakazawa H, Mori H (2003) Biodegradable gelatin hydrogel potentiates the angiogenic effect of fibroblast growth factor 4 plasmid in rabbit hindlimb ischemia. J Am Coll Cardiol 41:1056–1062
18. Xie Y, Yang ST, Kniss DA (2001) Three-dimensional cell-scaffold constructs promote efficient gene transfection: implications for cell-based gene therapy. Tissue Eng 7:585–598
19. Panetta CJ, Miyauchi K, Berry D, Simari RD, Holmes DR, Schwartz RS, Caplice NM (2002) A tissue-engineered stent for cell-based vascular gene transfer. Hum Gene Ther 13:433–441
20. Gidh-Jain M, Huang B, Jain P, el-Sherif N (1996) Differential expression of voltage-gated K+ channel genes in left ventricular remodeled myocardium after experimental myocardial infarction. Circ Res 79:669–675
21. Takeshita S, Zheng LP, Brogi E, Kearney M, Pu LQ, Bunting S, Ferrara N, Symes JF, Isner JM (1994) Therapeutic angiogenesis. A single intraarterial bolus of vascular endothelial growth factor augments revascularization in a rabbit ischemic hind limb model. J Clin Invest 93:662–670
22. Ribeiro RA, Flores CA, Cunha FQ, Ferreira SH (1991) IL-8 causes in vivo neutrophil migration by a cell-dependent mechanism. Immunology 73:472–477
23. Fukuyama N, Ichimori K, Su Z, Ishida H, Nakazawa H (1996) Peroxynitrite formation from activated human leukocytes. Biochem Biophys Res Commun 224:414–419
24. Mori H, Haruyama S, Shinozaki Y, Okino H, Iida A, Takanashi R, Sakuma I, Husseini WK, Payne BD, Hoffman JI (1992) New nonradioactive microspheres and more sensitive X-ray fluorescence to measure regional blood flow. Am J Physiol 263:H1946–H1957
25. Nagaya N, Kangawa K, Kanda M, Uematsu M, Horio T, Fukuyama N, Hino J, Harada-Shiba M, Okumura H, Tabata Y, Mochizuki N, Chiba Y, Nishioka K, Miyatake K, Asahara T, Hara H, Mori H (2003) Hybrid cell-gene therapy for pulmonary hypertension based on phagocytosing action of endothelial progenitor cells. Circulation 108: 889–895
26. Kobinger GP, Deng S, Louboutin JP, Vatamaniuk M, Matschinsky F, Markmann JF, Raper SE, Wilson JM (2004) Transduction of human islets with pseudotyped lentiviral vectors. Hum Gene Ther 15:211–219
27. Leonard EJ, Yoshimura T (1990) Human monocyte chemoattractant protein-1 (MCP-1). Immunol Today 11:97–101
28. Ikeda Y, Young LH, Lefer AM (2002) Attenuation of neutrophil-mediated myocardial ischemia-reperfusion injury by a calpain inhibitor. Am J Physiol Heart Circ Physiol 282:H1421–H1426
29. Veit K, Boissel JP, Buerke M, Grosser T, Meyer J, Darius H (1999) Highly efficient liposome-mediated gene transfer of inducible nitric oxide synthase in vivo and in vitro in vascular smooth muscle cells. Cardiovasc Res 43:808–822
30. Maasho K, Marusina A, Reynolds NM, Coligan JE, Borrego F (2004) Efficient gene transfer into the human natural killer cell line, NKL, using the Amaxa nucleofection system. J Immunol Methods 284:133–140
31. Mertz KD, Weisheit G, Schilling K, Luers GH (2002) Electroporation of primary neural cultures: a simple method for directed gene transfer in vitro. Histochem Cell Biol 118:501–506
32. Lei Y, Haider HK, Shujia J, Sim ES (2004) Therapeutic angiogenesis; Devising new strategies based on past experiences. Basic Res Cardiol 99:121–132
33. Ott HC, McCue J, Taylor DA (2005) Cell-based cardiovascular repair: The hurdles and the opportunities. Basic Res Cardiol 100:504–517
34. Koch KC, Schaefer WM, Liehn EA, Rammos C, Mueller D, Schroeder J, Dimassi T, Stopinski T, Weber C (2006) Effect of catheter-based transendocardial delivery of stromal cell-derived factor 1α on left ventricular function and perfusion in a porcine model of myocardial infarction. Basic Res Cardiol 101:69–77

FEBS Letters 581 (2007) 2416–2422

Crystal structures of catrocollastatin/VAP2B reveal a dynamic, modular architecture of ADAM/adamalysin/reprolysin family proteins

Tomoko Igarashi[a], Satohiko Araki[b], Hidezo Mori[a], Soichi Takeda[a,*]

[a] *Department of Cardiac Physiology, National Cardiovascular Center Research Institute 5-7-1 Fujishiro-dai, Suita, Osaka 565-8565, Japan*
[b] *Sugashima Marine Biological Laboratory, Graduate School of Science, Nagoya University, Toba, Mie 517-0004, Japan*

Received 26 January 2007; revised 29 March 2007; accepted 20 April 2007

Available online 30 April 2007

Edited by Christian Griesinger

Abstract **Catrocollastatin/vascular apoptosis-inducing protein (VAP)2B is a metalloproteinase from *Crotalus atrox* venom, possessing metalloproteinase/disintegrin/cysteine-rich (MDC) domains that bear the typical domain architecture of a disintegrin and metalloproteinase (ADAM)/adamalysin/reprolysin family proteins. Here we describe crystal structures of catrocollastatin/VAP2B in three different crystal forms, representing the first reported crystal structures of a member of the monomeric class of this family of proteins. The overall structures show good agreement with both monomers of atypical homodimeric VAP1. Comparison of the six catrocollastatin/VAP2B monomer structures and the structures of VAP1 reveals a dynamic, modular architecture that may be important for the functions of ADAM/adamalysin/reprolysin family proteins.**

Keywords: ADAM; Adamalysin; Reprolysin; MDC protein; Metalloproteinase disintegrin; Apoptotic toxin

1. Introduction

Hemorrhagic snake venoms induce local and systemic hemorrhaging by disrupting the walls of the blood vessels in envenomed patients [1]. In vitro, they induce apoptosis specifically in cultured vascular endothelial cells [2]. Vascular apoptosis-inducing protein (VAP)1 and VAP2 were originally isolated from *Crotalus atrox* venom [3,4], and similar apoptotic toxins have been isolated from other snake venoms [5–7]. VAP1 is a disulfide-bridged homodimeric protein with an apparent molecular weight of 110 kDa, and an isoelectric point of 8.5. VAP2 is a single chain protein with a MW of 55 kDa and an isoelectric point of 4.5 [3,4,8]. VAPs are members of the P-III class of snake venom metalloproteinases (SVMPs), possessing a metalloproteinase/disintegrin/cysteine-rich (MDC) domain architecture typical of a disintegrin and metalloproteinase (ADAM)/adamalysin/reprolysin family proteins [9,10]. VAP-induced apoptosis is dependent on its catalytic activity [8], is inhibited by antibodies to integrins α3, α6, β1 and CD9 [11], and involves activation of specific caspases [12]. However, the physiological targets of VAPs and the underlying mechanism of VAP-induced apoptosis remain elusive.

ADAMs are a family of mammalian membrane-anchored glycoproteins that have been implicated in the processing of cell surface and extracellular matrix proteins [13,14]. The crystal structures of several P-I class SVMPs, which contain only a metalloproteinase (M)-domain, and the isolated M and disintegrin/cysteine-rich (DC) domains of ADAMs have been determined [15–18]. However, structures of ADAM/adamalysin/reprolysin family proteins that include the entire MDC domain have not been determined. The relevance of the multidomain structure to the catalytic and adhesive functions of this family of proteins is an important issue that remains to be elucidated. To better understand the structure–function relationship of ADAM/adamalysin/reprolysin family proteins, and how it relates to the molecular mechanism of VAP-induced apoptosis, we have been engaged in crystallographic studies of VAPs. Recently, we determined the crystal structure of VAP1, revealing the MDC domain architecture for the first time [19]. Although the intrinsic two-fold symmetry of atypical homodimeric VAP1 conferred a great advantage for both its crystallization and structural resolution, the possibility remained that the spatial arrangement of the MDC domains of VAP1 differed from that of monomeric SVMPs and ADAMs, due to crystallographic restraints imposed on the molecule. The majority of ADAMs and SVMPs do not to form VAP1-type dimers, most likely due to the lack of a consensus QDHSK sequence [19] (residues 320–324 in VAP1, in which the Nζ atom of Lys324 is coordinated by the six oxygen atoms of another monomer and plays a pivotal role in dimer formation), and Cys365, which are conserved among the dimeric SVMPs (Supplementary Fig. 1). Therefore, to elucidate the general architecture of proteins of the ADAM/adamalysin/reprolysin family, we crystallized VAP2 and determined its structure. We modeled all of the structures as monomers of VAP2B, which is identical to catrocollastatin, a protein previously isolated as a platelet aggregation inhibitor [20]. Here we describe the structure of catrocollastain/VAP2B, as determined in three different crystal forms. These are the first reported crystal structures of the monomeric class of proteins in ADAM/adamalysin/reprolysin family.

2. Materials and methods

Protein preparation and crystallization were performed as previously described [21]. The diffraction data sets were collected at the

*Corresponding author. Fax: +81 6 6872 7485.
E-mail address: stakeda@ri.ncvc.go.jp (S. Takeda).

Abbreviations: ADAM, a disintegrin and metalloproteinase; MDC, Metalloproteinase/disintegrin/cysteine-rich; SVMP, Snake venom metalloproteinase; HVR, Hyper-variable-region; ncs, Non-crystallographic symmetry; VAP, Vascular apoptosis-inducing protein; PEG, Polyethyleneglycol

0014-5793/$32.00
doi:10.1016/j.febslet.2007.04.057